Preferential transport of nitrate to a tile drain in an intermittent-flood-irrigated field: Model development and experimental evaluation

B. P. Mohanty

U.S. Salinity Laboratory, Riverside, California

R. S. Bowman and J. M. H. Hendrickx

Department of Earth and Environmental Sciences, New Mexico Institute of Mining and Technology, Socorro

J. Simunek and M. T. van Genuchten

U.S. Salinity Laboratory, Riverside, California

Abstract. A comprehensive field experiment was conducted near Las Nutrias, New Mexico, to study field-scale flow and transport in the vadose zone. The field data were analyzed in terms of a two-dimensional numerical model based on the Richards equation for variably saturated water flow, convection-dispersion equations with first-order chemical decay chains for solute transport, and bimodal piecewise-continuous unsaturated hydraulic functions to account for preferential flow of water and nitrate-nitrogen (NO_3-N; loosely used as NO_3^-) following flood irrigation events at the experimental site. The model was tested against measured NO_3^- flux concentrations in a subsurface tile drain, several monitoring wells and nested piezometers, and against resident NO_3^- concentrations in the soil profile (obtained at 52 spatial locations and four depths along a transect). NO_3^- transport at the field site could be described better with the bimodal hydraulic functions than using the conventional approach with unimodal van Genuchten-Mualem type hydraulic functions. Average resident nitrate concentrations measured across the soil profile were predicted reasonably well. However, NO_3^- flux concentrations in the subsurface tile drain and piezometers at the field site were occasionally underestimated or overestimated depending upon the irrigation sequence in three field benches, probably reflecting unrepresented three-dimensional regional flow/transport processes. Limiting the capture zone to a region closer to the tile drain did lead to a better match with observed sharp increases and decreases in predicted NO_3^- flux concentrations during the irrigation events. On the basis of this result we inferred that the preferential flow intercepted by the tile drain was generated in close proximity of the drain and essentially oriented vertically. In summary, our study suggests that irrigation scheduling in adjacent field plots, drainage design (e.g., spacing between tiles, drain depth, drain diameter) and effectiveness (e.g., drain blockage), preferential flow in (horizontal) surface-opened shallow cracks and (vertical) macropores, and transient regional groundwater flow can add significant uncertainty to the predictions of (local-scale) flow and transport to a tile drain.

1. Introduction

Field-scale transport of agricultural chemicals from the soil surface to and into groundwater through the vadose zone is increasingly recognized as an extremely complicated process. Available computer models generally lack one or several of the most important physical, chemical, or biological processes operative at the field scale. One such important field-scale process is the preferential flow of water and dissolved constituents through a complex network of soil macropores, worm holes, root channels, and structural cracks, especially during and after the application of large amounts of water. Furthermore, processes occurring at larger (e.g., regional) scales may add significant uncertainty to the predictions based on local-scale

physical, chemical, and biological process information. Deterministic identification and representation of the most relevant flow and transport processes under site-specific soil, crop, water, and chemical management conditions and for the prevailing atmospheric, topographic, and hydrologic situations should optimally be done through well-designed field experiments and modeling in an interactive manner [*Tod and Grismer*, 1996]. Site-specific findings should be assimilated later to deduce more general rules.

Tile drains are popularly used in many agricultural fields for draining excess water from the vadose zone to sustain optimum soil water contents for crop production and/or maintaining low levels of soil salinity, sodicity, or other contaminants. Tile drains have been used recently to advantage for studying field-scale transport behavior [*Hallberg et al.*, 1986]. In different studies [*Shalit and Steenhuis*, 1996; *Singh et al.*, 1996; *Munster et al.*, 1996, 1994; *Booltink*, 1995; *Kladivko et al.*, 1991; *Czapar and*

Plate 1. Areal view of the Las Nutrias field site. Numbers along the bench boundaries indicate monitoring wells and piezometers (asterisks). Collector drain along the west boundary of the west bench, piezometer nests (32 and 34), and monitoring well (33) are outside the snap shot boundary.

Kanwar, 1991; *Richard and Steenhuis*, 1988; *Bowman and Rice*, 1986; *White et al.*, 1983], researchers have interpreted sharp increases in tile drain outflow and its chemical concentrations, during and following heavy irrigation or rainfall, as being indicative of field-scale preferential flow. Moreover, many studies claim that tile drains are good spatial integrators of field-scale flow and chemical transport processes (including preferential flow) and hence that they are excellent tools for estimating effective flow and transport properties of relatively large fields. A limited number of two-dimensional numerical modeling studies [e.g., *Khan and Rushton*, 1996a; *Munster et al.*, 1996; *Singh et al.*, 1996; *Singh and Kanwar*, 1995a, b; *Kamra et al.*, 1991a, b; *Sanoja et al.*, 1990] have tested the use of tile drains as spatial integrators of matrix-dominated flow in the presumed absence of preferential flow. Also, *Jury* [1975a, b] developed an analytical method to calculate travel times for flow originating at different distances from a tile drain using the assumption of Darcian flow. Attempts to test models with field data [e.g., *Ragab et al.*, 1996; *Singh and Kanwar*, 1995a, b; *Kamra et al.*, 1991b] often were not successful because of a failure to account for preferential flow and/or transient regional groundwater flow. These studies all assumed that the capture zone of the tile drain remained constant with time, irrespective of the presence or absence of matrix, preferential, or regional flow regimes at the experimental site. Other studies by *Luxmoore* [1991] and *Thomas and Barfield* [1974] concluded that tile drains can be unreliable for quantifying chemical transport from a field since they intercept only a relatively small proportion of the total flow in the field. The above findings are partly due to our still limited capability to accurately measure and model multidimensional field-scale water flow and solute transport under variably saturated conditions, especially during conditions of preferential flow.

In a recent paper, *Mohanty et al.* [1997] identified and modeled preferential flow to a tile drain in a macroporous field under intermittent flood irrigation practice near Las Nutrias, New Mexico. Preferential flow was modeled by using bimodal type piecewise-continuous unsaturated hydraulic functions. Results of the study showed that the bimodal functions did lead to better predictions of the drainage flux in the subsurface tile drain following any irrigation event as compared to the unimodal van Genuchten-Mualem hydraulic functions. In this paper we will further evaluate the bimodal hydraulic functions with regard to predicting field-scale preferential solute transport under intermittent flood irrigation. Specific objectives are (1) to monitor and interpret transient resident NO_3^- concentrations at different spatial locations and depths across the vadose zone, (2) to monitor and analyze NO_3^- flux concentration in a subsurface tile drain, in several monitoring wells, and in nested piezometers at the experimental field, (3) to develop a two-dimensional numerical model for preferential flow and transport following flood irrigation using the piecewise-continuous hydraulic functions, (4) to test model performance using the observed NO_3^- flux and resident concentrations, and (5) to investigate the appropriateness of tile drains as field integrators of flow and transport for the specific preferential and regional groundwater flow conditions characteristic of our experimental site.
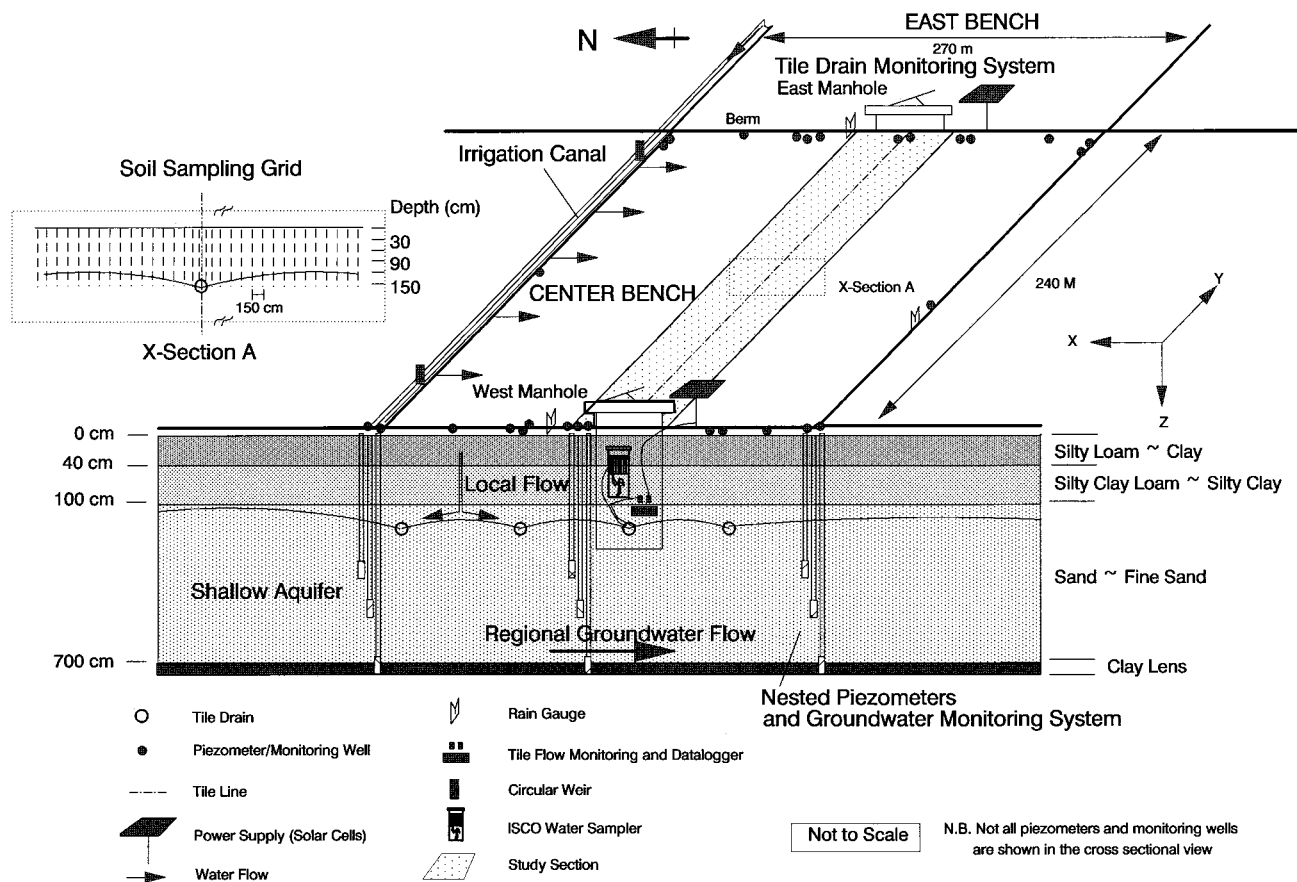
2. Field Site

The experimental field site is located on a 24-ha commercial agricultural farm, situated on an alluvial flood plain of the Rio Grande, near Las Nutrias, New Mexico. The basin lies within the Rio Grande rift, a series of north-south trending half grabens oriented parallel to the Rio Grande. The climate is arid to semiarid and has a wide range in temperature and rainfall. The parent material for the entire valley is alluvium. Plate 1 [*Mohanty et al.*, 1997] shows the major soil classes across the 6-ha center bench of the field, including our study section. In general, the field site consists of silty clay loam sediments with moderate to poor drainage properties underlain by fine sands, with no impeding strata to a depth of about 7 m [*National Resource Conservation Service* (*NRCS*), 1992]. Surface horizons, however, contain visible root channels, worm holes, and cracks, thus potentially providing a complex network of preferential flow paths. The field (Plate 1) is relatively flat and divided into three benches: east (240 m × 270 m), center (240 m × 270 m), and west (420 m × 270 m), separated by berms. To sustain agricultural productivity, the field site was equipped with surface irrigation and subsurface (tile) drainage systems.

The subsurface tile drainage system consisted of four lateral drain lines installed at a depth of ~1.2 m. The tile drains connected to a main drain line leading to an off-site open-channel drain on the west. Irrigation return flows draining from the field, as well as periodic buildup of shallow groundwater flowing in from off-site areas, were collected by the drainage system. A southern section of the center bench drainage system was isolated by installing two manholes along a single drain line at the east (up) and west (down) ends of the bench (Plate 1 and Figure 1). The manholes allowed regular sampling of water quantity and quality entering and leaving the study section of the drain line. The manholes were equipped with Signet® flow measurement systems including data loggers for monitoring flow rates at 5-min intervals. Automated ISCO® 2700 samplers were used to collect drain water samples in these manholes. We used the isolated section of the center bench for collecting soil hydraulic parameters and for monitoring flow and transport in the vadose zone. Horizontal and vertical pressure gradients and chemical concentrations of groundwater at different (2, 3, 5, and 7 m) depths in the underlying aquifer were determined regularly using piezometers and observation wells along the periphery of the field site. For this purpose, eight nested piezometers at 2-, 3-, 5-, and 7-m depths and 34 monitoring wells at 2-m depth (Plate 1) were installed around the field. Three rain gauges were located on the center bench to monitor the average precipitation input of individual rainfall events.

A concrete-lined canal on the north side of the field supplied irrigation water to all three benches through a number of control gates using flood irrigation. Irrigation water flowed from the north end of the field to the south end in about 4–7 hours and remained ponded in the field for several hours with simultaneous infiltration. After the desired amount of water was delivered to the field, irrigation supply was cutoff, thus allowing continued variably saturated flow and redistribution within the soil profile. A 25-cm-diameter circular weir of the type developed by *Samani* [1993] was used in the irrigation canal to measure water input to the center bench during each irrigation event. The local farmer scheduled the water input events to different benches depending on the consumptive needs of his crops at the different growth stages. Table 1 shows the irrigation dates and amounts, including the bench sequence during 1994 and 1995. All three benches normally received water on the same day, although irrigation in the three benches was spread occasionally over 2-day periods. Table 2 shows the

Figure 1. Three-dimensional view of the field site including hydrology, soil and water quality monitoring facilities, and locations of surface and subsurface site characterization studies.

crop rotation for 1994/1995. Details of the measurement and mathematical description of the surface and shallow subsurface hydraulic properties of the field site are given by *Mohanty et al.* [1997].

2.1. Solute Flux Concentration Sampling

Observation wells at 2-m depth and piezometers at 2-, 3-, 5-, and 7-m depths (Plate 1 and Figure 1) were sampled intermittently for chemical concentrations to determine the spatiotemporal distributions and vertical concentration gradients of solutes in the shallow groundwater zone. Sampling intervals ranged from a few weeks during summer to a few months

during winter. To avoid measuring stagnant well water, approximately five well volumes were bailed before samples were actually collected. A total of 544 and 416 water samples were collected during 1994 and 1995, respectively. ISCO 2700 automatic water samplers were used to collect tile effluents at the east and west manholes (Plate 1 and Figure 1). During irrigations, water samples were taken every 2 hours for the first 48 hours, then once every 4 hours for the next 48 hours, and subsequently once every 6 hours for 72 hours. This scheme was followed by sampling at 24-hour intervals until the next irrigation. Water samples collected from the tile drains, monitoring wells, and piezometers were later analyzed for NO_3^- and other

Table 1. Irrigation Application Dates and Volumes Applied to the Center Bench

Date	Day*	Total Elapsed Time, hours	Total Volume, L	Total Depth, mm	Bench Sequence†
June 8, 1994	721	4.5	4.14E + 06	61.22	E-C-W
June 27, 1994	740	7.0	4.56E + 06	67.43	E-C-W
Aug. 8, 1994	782	6.0	5.10E + 06	75.41	E-C-W
Sept. 28, 1994	833	7.5	5.88E + 06	86.93	W-C-E
April 10, 1995	1026	6.0	6.47E + 06	95.76	E-W-C
April 26, 1995	1043	6.5	5.37E + 06	79.48	E-W-C

Bench sequence indicates the order of water application during a particular irrigation event. Irrigation events prior to June 1994 were not recorded. Read 4.14E+06 as 4.14×10^6.

*Sequential day from the start of the project.

†E, east bench; C, center bench; W, west bench.

solutes by using High Performance Liquid Chromatography (HPLC) in the New Mexico Institute of Mining and Technology soil water chemistry laboratory.

Table 3 presents mean NO_3^- flux concentrations for the 34 observation wells located at the experimental field site. No general trend was found in the mean concentrations in horizontal space. The NO_3^- distributions were somewhat influenced by the irrigation sequence and timing of the three field benches (to be discussed in section 4) and by spatial variability in the flow/transport process. However, mean NO_3^- flux concentration showed a somewhat decreasing trend with time. Except for a few hot points having high values (~7 mg/L), NO_3^- concentrations were generally quite low across the field at 2-m depth on all sampling dates. No apparent reason could be found for the localized hot points. Figure 2 shows the vertical profile in the NO_3^- flux concentration on different dates measured in four nested piezometers (11, 14, 21, and 24, Plate 1) located on the four corners of our study section.

Table 2. Crop Rotation Schedule for the Center Bench at the Las Nutrias Field Site

Crop	Planting Date	Harvest Dates
Winter wheat	Oct. 10, 1993	not harvested
Sorghum-Sudan cross	May 13, 1994	July 19, 1994
Alfalfa	Sept. 25, 1994	May 29, 1995
		June 2, 1995
		July 5, 1995
		Aug. 6, 1995
		Sept. 6, 1995
		Oct. 15, 1995

Except for one outlier, no significant vertical concentration gradient (between 2- and 7-m depths) was found in the shallow groundwater zone. Moreover, NO_3^- flux concentration at these depths remained low and approximately unchanged through-
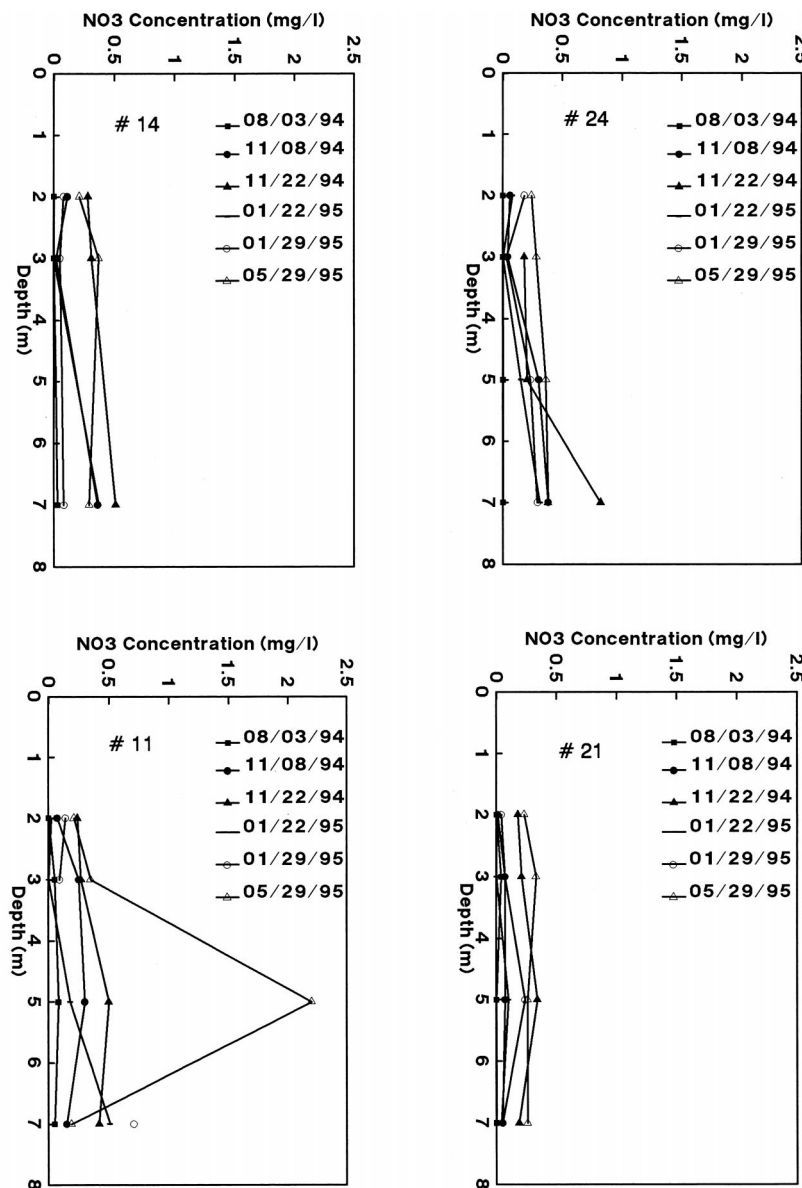
Figure 2. Intermittent NO_3^- flux concentrations observed in the piezometers on the four corners of the study section in the center bench.

Table 3. NO$_3^-$ Flux Concentration in the Monitoring Wells at the Las Nutrias Field Site in 1994

| Well	Easting	Northing	April 1	April 10	April 24	April 29	May 17	May 25	June 1	June 9	July 1	July 19	Aug. 19	Sept. 11	Sept. 24	Oct. 8	Oct. 23	Nov. 8	Nov. 15	Mean
A1	1583.6	354.8	0.926	2.725	1.370	1.230	0.950	0.900	1.160	2.740	1.860	2.660	1.560	2.770	1.650	0.46	0.547	0.904	0.100	1.44
A2	1558.3	221.6	0.000	0.149	0.200	0.260	0.200	0.210	0.190	0.390	0.030	0.170	0.080		0.010	0.13	0.188	0.048	0.234	0.16
A3	1532.3	96.21	2.438	1.084	0.130	0.160	0.080	0.070	0.000	0.450	0.050	0.080	0.080	1.680	0.070	0.03	0.146	0.051	0.185	0.40
A4	1460.7	377.2				7.000	7.000	7.000	7.000	0.390	0.030	0.060	0.000	0.000	0.490	0.03	0.243	0.654	1.484	2.24
A5	1428.8	119.9	0.000	0.923	6.280	2.460	0.320	0.330	0.350	1.720	3.130	1.280	7.000	0.310	0.310	0.30	0.109	0.023	0.043	1.46
A6	1329	396.8	0.000	0.056	0.210	0.070	0.060	0.090	0.000	0.150	0.030	0.030	0.000	0.000	0.020	0.01	0.129	0.164	0.102	0.07
A7	1314.4	279.3			2.560	2.810	1.370	0.150	0.100	0.560	0.070	0.030	0.000	0.000	0.410	0.04	0.110	0.032	0.125	0.56
A8	1298.7	150.7	3.801	0.176	0.560	0.210	7.540	0.100	0.070	0.300	1.950	0.030	0.020	0.000	0.120	0.03	0.074	0.042	0.017	0.88
A9	1325.6	397.5	0.050	0.065	0.180	0.180	0.070	0.090	0.080	0.040	0.070	0.030	0.000	0.780	0.200	0.24	0.138	0.030	0.033	0.13
A10	1314.9	316.1			0.160	0.090	0.080	0.090	0.000	0.530	0.040	0.000	0.000	0.000	0.040	0.02	0.129	0.026	0.017	0.09
A11	1310.4	278			0.190	0.130	0.060	0.100	0.000	0.220	0.040	0.030	0.000	0.010	0.030	0.01	0.325	0.065	0.085	0.09
A12	1306.2	245.8			0.220	0.110	0.060	0.100	0.000	0.250	0.040	0.020	0.000	0.200	0.070	0.02	0.116	0.012	0.124	0.10
A13	1305.7	242.1			0.190	0.100	0.110	0.110	0.080	0.520	0.050	0.030	0.000	0.000	0.050	0.01	0.000	0.052	0.134	0.10
A14	1301.7	208.8	0.233		0.210	0.160	0.100	0.080	0.000	0.270	0.060	0.030	0.000	0.000	0.050	0.00	0.170	0.113	0.121	0.10
A15	1297.3	173.7			0.210	0.130	0.120	0.080	0.070	2.180	0.000	0.030	0.020	0.000	0.060	0.01	0.000	0.088	0.117	0.21
A16	1294.6	151.6	4.621	0.603	0.110	0.130	0.100	0.090	0.000	0.080	0.140	0.020	7.000		0.050	0.00	0.014			0.93
A17	1208.8	420.9	0.072	0.072	0.270	0.050	0.120	0.160	0.140	0.300	0.060	0.030	0.000	0.020	0.070	0.01	0.030		0.345	0.11
A18	1153.5	183.8	0.221	0.117	0.210	0.090	0.090	0.090	0.000	0.550	0.060	0.000	7.000	0.000	0.050	0.15	0.148	0.047	0.111	0.53
A19	1088.6	436.6	0.027	0.079	0.190	0.050	0.090	0.090	0.080	0.120	0.040	0.030	0.690	0.000	0.050	0.51	0.572	0.072	0.385	0.18
A20	1077.8	365.9			0.310	0.190	0.110	0.090	0.000	0.120	0.030	0.040	0.000		0.050	0.04	0.097	0.062	0.128	0.09
A21	1072.4	328.9			0.420	0.080	0.090	0.070	0.000	0.120		0.090	0.000	0.000	0.060	0.01	0.007	0.007	0.117	0.08
A22	1067.5	296.3			0.170	0.090	0.110	0.080	0.000	0.300	0.320	0.040	0.040	0.030	0.080	0.01	0.023	0.041	0.108	0.10
A23	1066.8	292.2			0.280	0.050	0.120	0.080	0.080	1.450	0.030	0.000	0.040	0.000	0.080	0.01	0.000	0.048	0.036	0.15
A24	1062.3	261.6			0.290	0.140	0.120	0.070	0.000	1.840	0.000	0.000	0.000	0.000	0.130	0.01	0.038	0.062		0.19
A25	1056.7	223.5			0.190	0.050	0.120	0.760	0.090	0.780	0.000	0.050	0.030	0.000	0.090	0.03	0.414	0.158	0.109	0.19
A26	1054.2	207.7	0.140	0.059	0.210	0.080	0.110	0.090	0.070	0.010	0.230	0.050	0.040	0.000	0.090	0.01	0.057		0.153	0.09
A27	1083.2	438.5	0.824	1.454	1.280	1.720	0.580	0.090	0.430	0.140	4.000	0.040	0.000	0.000	0.070	0.05	0.105	0.060	0.033	0.64
A28	1067.9	328.1			0.190	0.120	0.120	0.080	0.080	7.000	0.000	0.000	0.000	0.000	0.080	0.01	0.044	0.102	0.065	0.53
A30				0.086	1.940	0.440	0.000	0.610	0.180	1.490	1.700	0.070	0.000	0.000	0.400	2.76		1.156	6.619	1.16
A32	583.8	526.6	0.181	0.097	0.260	0.090	0.120	0.100	0.000	0.040	0.000	0.040	0.000	0.000	0.090	0.04	0.000	0.050	0.033	0.07
A33	631	287.8	3.102	0.939	0.900	0.050	0.120	0.150	0.140	0.550	0.040	0.040	0.030	0.000	0.100	0.01	0.000	0.027	0.031	0.37
A34	660.2	298.3	1.853	0.047	0.050	0.230	0.110	0.110	0.070	0.170	0.000	0.070	0.000	0.000	0.120	0.01	0.000	0.022	0.036	0.17
Mean			1.088	0.514	0.643	0.586	0.636	0.385	0.327	0.805	0.455	0.160	0.738	0.201	0.164	0.16	0.128	0.145	0.374	

Concentrations are in milligrams per liter. Blank cells indicate that the data are missing.

out the sampling period (August 1994 to approximately May 1995).

NO_3^- flux concentration in the tile drain water collected from the east and west manholes are shown in Figure 3. Evidently, in both manholes, sharp increases in the drainage water NO_3^- concentrations occurred within a few hours following all irrigation events. The concentrations remained high for a few days, followed by sharp drops (with little tailing) to the relatively low background preirrigation concentration level. In general, NO_3^- concentration in the tile water became as high as $10 \sim 15$ mg/L before returning to background levels of about $0.3 \sim 0.5$ mg/L. The sharp increases and decreases in NO_3^- concentration qualitatively suggest that transport to the tile drain was mostly convection-dominated following the irrigation events.

2.2. Solute Resident Concentration Sampling

From late February thru early March 1994 and 1995, soil samples were collected from the center bench study section along a north-south transect perpendicular to the tile drain, as shown in Figure 1. Fifty sampling sites along this transect were arranged 1.5 m apart on both sides of the tile drain. In addition, several soil samples were collected very close to the tile drain. An ~2-m separation distance was maintained between
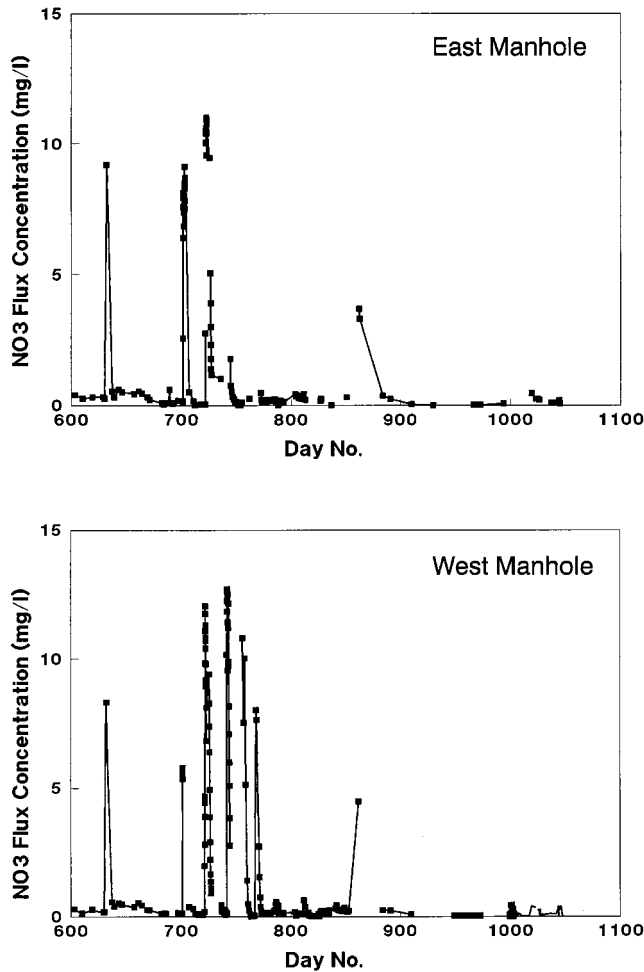
Figure 3. Tile flux NO_3^- concentrations at the east and west manholes. Breaks in the line indicate missing data because of human or instrumental factors.
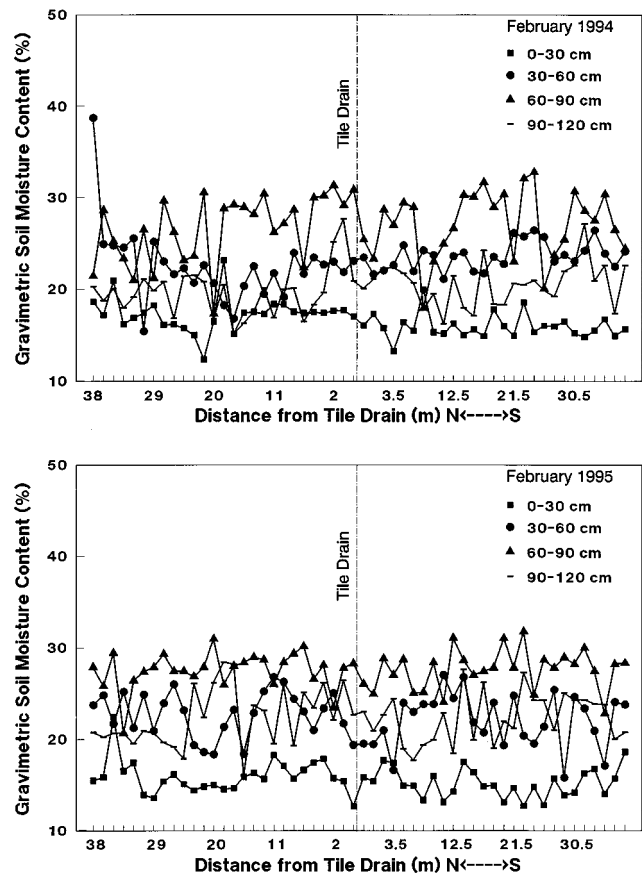

Figure 4. Profile soil moisture content across the N-S transect in February 1994 and February 1995 at the field site.

the 1994 and 1995 sampling transects. This sampling scheme was used to investigate possible spatial patterns (trends) in soil attributes (e.g., resident NO_3^- concentration) created as a result of flow to the tile drain. Soil samples were collected in 30-cm increments from the soil surface to a depth of 120 cm using Veihmeyer® soil sampling tubes. The soil samples were later analyzed for gravimetric soil water content, soil water NO_3^- concentration (by using HPLC), soil bulk density, and soil texture. Note that the same sites (within 1-m-diameter area) were previously also used for determining water retention and hydraulic conductivity functions using in situ and laboratory methods [*Mohanty et al.*, 1997].

Figures 4 and 5 show spatial distributions of the soil water content and the resident NO_3^- concentration at different depths across the north-south transect for February 1994 and 1995, respectively. Except for a narrow sharp dip in concentration near the tile drain in 1995, no plot-scale tile flow induced trend was found in the resident NO_3^- concentration at all four depths. This feature may indicate in part that the radial/vertical capture zone for the tile drain was quite narrow. Moreover, geostatistical analyses [*Journel and Huijbregts*, 1978] of the spatial data resulted in white noise dominated semivariograms (Figure 6) indicating no spatial structure. Table 4 gives descriptive statistics including mean, range, standard deviation, and W statistics [*Shapiro and Wilk*, 1965] of the 1994 and 1995 resident nitrate concentration and soil water content data. The concentration and soil water content data were both found normally distributed at all depths and times. The high
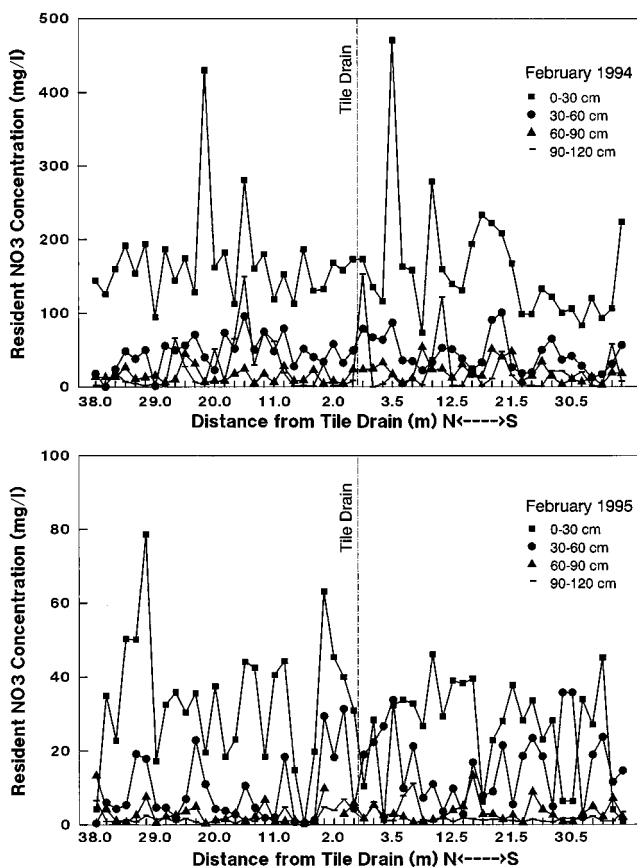
Figure 5. Profile resident NO_3^- concentrations across the N-S transect in February 1994 and February 1995 at the field site.
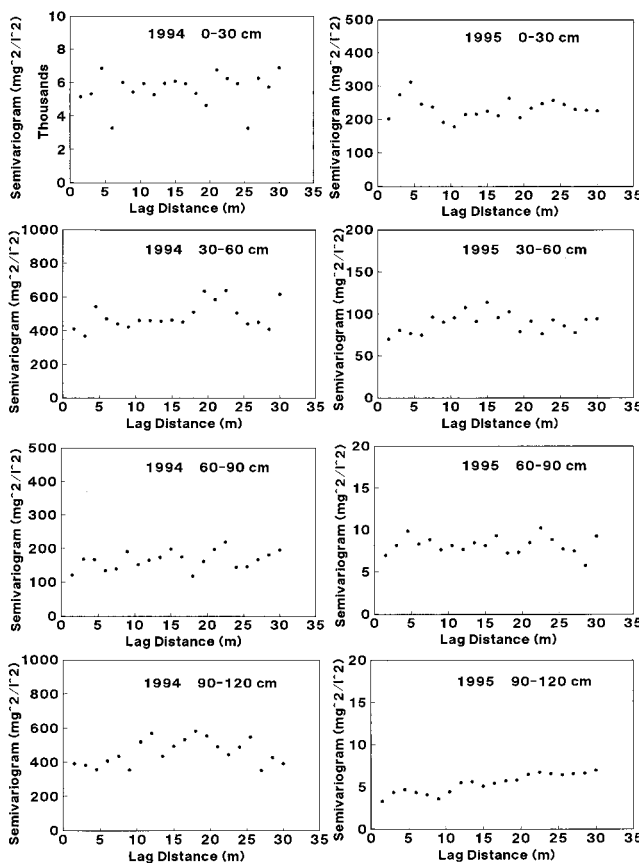
Figure 6. Semivariograms of profile resident NO_3^- concentrations in 1994 and 1995.

resident nitrate concentrations near the soil surface (0–30 cm) in 1994 were partly due to failure of winter wheat in the preceding season, which left large amounts of unused urea fertilizer in the soil. Furthermore, freezing of the surface soil during the winter months of 1993–1994 may have helped to preserve the NO_3^- until spring 1994. A statistical comparison showed significant differences between resident NO_3^- concen-

trations in 1994 and 1995, indicating its depletion from the soil profile over several crop growing seasons during the 1-year period. Depletion of NO_3^- was likely due to several simultaneous processes including convective-dispersive transport to groundwater, immobilization to biomass (i.e., organic nitrogen), denitrification to nitrogen gas, and uptake by plants. Total nitrate depletion was maximum near the soil surface (at 0–30 cm) and decreased gradually with depth. Low and statis-

Table 4. Descriptive Statistics of Resident NO_3^- Concentration and Soil Moisture Content at the Field Site in 1994 and 1995

	1994				1995			
Statistics	0–30 cm	30–60 cm	60–90 cm	90–120 cm	0–30 cm	30–60 cm	60–90 cm	90–120 cm
	Resident NO_3^- Concentration, mg/L							
Number	54	54	54	54	54	54	53	54
Mean	163.75	45.28	17.74	23.14	29.29	12.42	3.11	2.01
Standard deviation	72.23	23.10	12.54	35.25	15.88	10.06	2.98	2.13
Minimum	73.03	0.00	2.79	0.17	0.04	0.31	0.23	0.00
Maximum	470.82	100.87	53.27	153.29	78.51	35.74	13.20	11.03
W statistics*	0.775	0.97	0.874	0.664	0.964	0.889	0.795	0.365
	Gravimetric Soil Moisture Content, %							
Number	54	54	54	54	54	54	54	54
Mean	16.61	23.09	26.89	20.11	15.56	22.42	27.59	22.38
Standard deviation	1.77	3.10	3.71	2.56	1.74	2.74	2.09	2.97
Minimum	12.36	15.41	17.31	15.09	12.68	15.81	20.64	16.04
Maximum	23.15	38.73	32.78	27.68	22.40	27.03	31.77	28.45
W statistics*	0.938	0.829	0.936	0.954	0.943	0.957	0.950	0.964

*Normally distributed at a confidence level >0.9.

tically similar mean soil water contents during the 1994 and 1995 soil sampling events (Table 4) facilitated an unbiased year-to-year comparison of resident NO_3^- concentrations in the soil profile.

3. Model Description

The field experimental data were analyzed in terms of a two-dimensional numerical model accounting for variably saturated flow, convective-dispersive transport of several nitrogen species, and preferential flow/transport using bimodal type hydraulic functions. The model is a modification and extension of the CHAIN_2D code documented by *Simunek and van Genuchten* [1994]. This section gives a brief overview of the model.

3.1. Governing Equations for Water Flow and Solute Transport

Considering two-dimensional isothermal Darcian flow of water and assuming that the different pore regions (micropores and macropores) are at hydraulic equilibrium in a variably saturated rigid porous medium, the governing flow equation is given by the following modified form of the Richards equation:

$$\frac{\partial \theta}{\partial t} = \frac{\partial}{\partial x_i}\left[K\left(K_{ij}^A \frac{\partial h}{\partial x_j} + K_{iz}^A \right)\right] - S \qquad (1)$$

where θ is the volumetric water content $[L^3 L^{-3}]$, h is the pressure head $[L]$, S is a sink term $[T^{-1}]$, x_i ($i = 1, 2$) are the spatial coordinates $[L]$, t is the time $[T]$, K_{ij}^A are components of a dimensionless anisotropy tensor K^A, and K is the unsaturated hydraulic conductivity function $[LT^{-1}]$ given by

$$K(h, x, z) = K_s(x, z) K_r(h, x, z) \qquad (2)$$

where K_r is the relative hydraulic conductivity and K_s is the saturated hydraulic conductivity $[LT^{-1}]$. The anisotropy tensor K_{ij}^A in (1) is used to account for an anisotropic medium. The diagonal entries of K_{ij}^A equal 1 and off-diagonal entries zero for an isotropic medium. If (1) is applied to planar flow in a vertical cross section, $x_1 = x$ is the horizontal coordinate and $x_2 = z$ is the vertical coordinate, the latter taken to be positive upward. Einstein's summation convention is used in (1). Hence when an index appears twice in an algebraic term, this particular term must be summed over all possible values of the index.

Piecewise-continuous hydraulic functions [*Mohanty et al.*, 1997] were found to perform better than the normal unimodal hydraulic functions when simulating water flow at our experimental field site. For a multimodal pore-size distribution containing p capillary-dominated flow domains, the piecewise-continuous soil water retention and hydraulic conductivity functions can be written as

$$\theta(h) = \sum_p w_p \theta_p(h) = \sum_p w_p \left[\theta_{r,p} + \frac{\theta_{s,p} - \theta_{r,p}}{[1 + (\alpha_p h)^{n_p}]^{m_p}}\right] \qquad (3)$$

$$h \leq h_\theta^*$$

$$\theta = \theta_{s(p=1)} \qquad h > h_\theta^* \qquad (4)$$

$$K(h) = \sum_p k_p K_p(h)$$

$$= \sum_p k_p \frac{(1 - (\alpha_p h)^{n_p - 1}[1 + (\alpha_p h)^{n_p}]^{-m_p})^2}{[1 + (\alpha_p h)^{n_p}]^{m_p/2}}$$

$$(m_p = 1 - 1/n_p) \qquad h \leq h_K^* \qquad (5)$$

$$K_{np}(h) = K^* + K^*[\exp^{(h - h^*)\delta} - 1] \qquad h_K^* < h \leq 0 \quad (6)$$

$$K_{np}(h) = K^* + K^*[\exp^{(-h^*)\delta} - 1] \qquad h > 0 \qquad (7)$$

where K_p is the hydraulic conductivity of the pth capillary-dominated flow domain $[LT^{-1}]$, K_{np} is the hydraulic conductivity for noncapillary-dominated flow domain $[LT^{-1}]$, $\theta_{s,p}$ is the saturated water content of the pth capillary-dominated flow domain $[L^3 L^{-3}]$, $\theta_{r,p}$ is the residual water content of the pth capillary-dominated flow domain $[L^3 L^{-3}]$, h is the equilibrium soil water pressure head of the bulk soil across all flow domains $[L]$, $h_K^* \approx h_\theta^* = h^*$ is the critical or break point soil water pressure head where flow changes from capillary-dominated to noncapillary-dominated flow or vice versa $[L]$, K^* is the hydraulic conductivity corresponding to $h^*[LT^{-1}]$, δ is a fitting parameter representing effective macroporosity or other structural features contributing to noncapillary dominated flow $[L^{-1}]$, α_p, and n_p are fitting parameters [*van Genuchten*, 1980] for the pth capillary-dominated flow domain $[L^{-1}$, dimensionless], w_p is the weighting factor of the pth capillary-dominated flow domain such that $\sum w_p = 1$, and $0 \leq w_p \leq 1$ [dimensionless], and k_p is the saturated hydraulic conductivity for capillary-dominated flow domain p subjected to $\sum k_p = K^*[LT^{-1}]$.

Conceptually, the above functions indicate that the van Genuchten-Mualem models (equations (3) and (5)) should be used only for tensions greater than h^* when capillary flow dominates, in conjunction with other more appropriate models (e.g., equations (4) and (6)) for soil water retention and especially the hydraulic conductivity at tensions less than h^* when gravity flow dominates. Note that when $p = 1$, the sum type multimodal van Genuchten-Mualem hydraulic functions (equations (3) and (5)) reduce to the original unimodal van Genuchten-Mualem functions.

The partial differential equations governing two-dimensional equilibrium transport of solutes involved in a sequential first-order decay chain during transient water flow in variably saturated rigid porous medium are taken as [*Simunek and van Genuchten*, 1994]

$$\frac{\partial \theta c_1}{\partial t} + \frac{\partial \rho s_1}{\partial t} + \frac{\partial a_v g_1}{\partial t} = \frac{\partial}{\partial x_i}\left(\theta D_{ij,1}^\omega \frac{\partial c_1}{\partial x_j}\right) + \frac{\partial}{\partial x_i}\left(a_v D_{ij,1}^g \frac{\partial g_1}{\partial x_j}\right)$$

$$- \frac{\partial q_i c_1}{\partial x_i} - S c_{r,1} - (\mu_{\omega,1} + \mu_{\omega,1}')\theta c_1 - (\mu_{s,1} + \mu_{s,1}')\rho s_1$$

$$- (\mu_{g,1} + \mu_{g,1}')a_v g_1 + \gamma_{\omega,1}\theta + \gamma_{s,1}\rho + \gamma_{g,1}a_v \qquad k = 1 \quad (8)$$

$$\frac{\partial \theta c_k}{\partial t} + \frac{\partial \rho s_k}{\partial t} + \frac{\partial a_v g_k}{\partial t} = \frac{\partial}{\partial x_i}\left(\theta D_{ij,k}^\omega \frac{\partial c_k}{\partial x_j}\right) + \frac{\partial}{\partial x_i}\left(a_v D_{ij,k}^g \frac{\partial g_k}{\partial x_j}\right)$$

$$- \frac{\partial q_i c_k}{\partial x_i} - S c_{r,k} - (\mu_{\omega,k} + \mu_{\omega,k}')\theta c_k - (\mu_{s,k} + \mu_{s,k}')\rho s_k$$

$$- (\mu_{g,k} + \mu_{g,k}')a_v g_k + \mu_{\omega,k-1}'\theta c_{k-1} + \mu_{s,k-1}'\rho s_{k-1}$$

$$+ \mu_{g,k-1}'a_v g_{k-1} + \gamma_{\omega,k}\theta + \gamma_{s,k}\rho + \gamma_{g,k}a_v \qquad (9)$$

$$k \in (2, \cdots, K)$$

where c, s, and g are solute concentrations in the liquid $[ML^{-3}]$, solid $[MM^{-1}]$, and gaseous $[ML^{-3}]$ phases, respectively; q_i is the ith component of the volumetric flux density $[LT^{-1}]$; μ_ω, μ_s, and μ_g are first-order rate constants for
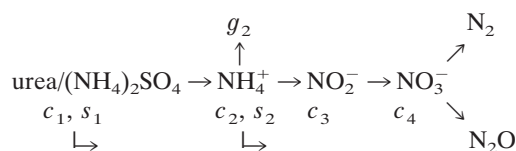
Table 5. Fertilization Applications at the Las Nutrias Field Site

Date	Day	Fertilizer	West Bench, kg/ha	Center Bench, kg/ha	East Bench, kg/ha
June 25, 1993	374	ammonium sulphate	448	448	⋯
Oct. 15, 1993	486	urea	224	⋯	⋯
Oct. 25, 1993	496	urea	⋯	224	⋯
March 7, 1994	628	ammonium sulphate	448	⋯	⋯
May 13, 1994	695	urea	224	⋯	⋯
April 3, 1995	1019	N(8)-P(36)-K(4)-S(4)	280	280	280

solutes in the liquid, solid, and gas phases $[T^{-1}]$, respectively; μ'_ω, μ'_s, and μ'_g are similar first-order reaction rate constants providing connections between the individual chain species; γ_ω, γ_s, and γ_g are zero-order rate constants for the liquid $[ML^{-3}T^{-1}]$, solid $[T^{-1}]$, and gas $[ML^{-3}T^{-1}]$ phases, respectively; ρ is the soil bulk density $[ML^{-3}]$, a_v is the air content $[L^3L^{-3}]$, S is the sink term in the water flow equation, c_r is the concentration of the sink term $[ML^{-3}]$, D_{ij}^ω is the dispersion coefficient tensor $[L^2T^{-1}]$ for the liquid phase; D_{ij}^g is the diffusion coefficient tensor $[L^2T^{-1}]$ for the gas phase; k represents the kth chain number; and K is the number of solutes involved in the chain reaction. The indicial notation used in this paper assumes summations over indices i and j (i, j) but not over index k.

3.2. Nitrogen Dynamics and Modeling

Novotny and Chesters [1981] summarized the complex behavior and transformation processes of nitrogen in soils. Fixation of atmospheric N, accumulation of ammonium-N, ammonification of organic-N, hydrolysis of urea, nitrification of ammonium-N, denitrification of nitrate-N, fixation of ammonium-N, plant uptake of nitrate-N, and ammonium volatilization constitute the most important transformation process of nitrogen in the soil-air-water-plant environment. Bacterial populations, soil temperature, soil water content, soil aeration, and soil pH are some of the factors that govern the transformation rates of nitrogen fertilizers to soluble nitrate-nitrogen and nitrogen gases. While in reality most of these nitrogen transformation processes will occur in a simultaneous and nonlinear fashion, we consider here only the most important forward processes, thereby keeping our model as simple as possible. Consistent with (7) and (8), nitrogen transformations were simulated by means of an apparent first-order decay chain in different phases as follows:

$$\begin{array}{ccccccc} & & g_2 & & & & N_2 \\ & & \uparrow & & & & \nearrow \\ \mathrm{urea/(NH_4)_2SO_4} & \rightarrow & NH_4^+ & \rightarrow & NO_2^- & \rightarrow & NO_3^- \\ c_1, s_1 & & c_2, s_2 & & c_3 & & c_4 \quad \searrow \\ \longmapsto & & \longmapsto & & & & N_2O \end{array}$$

where c, s, and g represent concentrations in the liquid, solid, and gaseous phases, respectively; straight arrows represent the different zero-order (γ) and first-order (μ, μ') rate reactions, and curved arrows indicate equilibrium distribution coefficients between phases. The approach lumps the processes of hydrolysis, nitrification, denitrification, volatilization, and plant uptake into a set of first- and zero-order reactions, while immobilization, mineralization, and biological fixation of nitrogen are considered unimportant during the study period.

Table 5 lists the fertilization schedule at our experimental field for 1993–1995. Ammonium sulphate and urea were the two most commonly used nitrogen fertilizers. Ammonium sulphate contains ~21% nitrogen by weight and is quite readily oxidized to NO_3^-. Urea, on the other hand, contains 45% nitrogen in organic form that first must be converted to ammonium before oxidation to nitrate can occur. This process is much slower, and hence urea-derived nitrogen will persist in the soil profile for much longer periods of time. Moreover, due to damage to the winter wheat crop in the fall of 1993, we anticipated that most of the urea remained unused at the field site until the spring of 1994.

The above set of flow and transport equations ((1), (8), and (9)) were solved using the Galerkin finite element method [*Simunek and van Genuchten*, 1994]. We used upstream weighting [*Yeh and Tripathi*, 1990] and an appropriate combination of space and time discretizations to adjust the local Peclet numbers and Courant numbers [*Perrochet and Berod*, 1993] for reducing undesired oscillations or numerical dispersion during convection-dominated transport. Convection was assumed to dominate transport processes during conditions of preferential flow following flood irrigation at the field site. For the numerical simulations we used a δ_θ convergence criterion [*Huang et al.*, 1996] in conjunction with the "mass conservative" modified Picard iteration method [*Celia et al.*, 1990] to enable relatively fast and robust convergence of the numerical solution.

3.3. Model Application to the Las Nutrias Field Site

Two-dimensional numerical simulations were carried out for a N-S vertical cross section across the center bench study section. The cross section was divided into 9350 nodes and 9126 quadrilateral elements as shown in Figure 7. On the basis of available surface infiltration and hydraulic property data, the soil profile was divided into three soil horizons characterized by three sets of field-averaged hydraulic functions. The three horizons were discretized into a total of 169 layers for numerical simulation purposes. Finer discretizations were used near the soil surface, across the horizon interfaces, and around the subsurface tile drain to handle relatively large local fluxes and pressure gradients in these areas. In addition, we kept our maximum vertical discretization relatively small ($\Delta z = 1$ cm) in the upper two horizons (to a depth of 100 cm). This finer discretization improved the numerical solutions, in particular, when the bimodal hydraulic functions were used. For the simulations we used a time-variant evapotranspiration rate assuming a normalized water uptake distribution across the top 40 cm of the soil profile in accordance with the approaches of *Feddes et al.* [1978] and *Simunek and van Genuchten* [1994]. Empirical functions [*Nielsen and MacDonald*, 1978] for NO_3^- uptake by different crops were used for the simulation. Measured resident NO_3^- concentrations before the 1994 crop growing season (i.e., February 1994) at different nodal points and
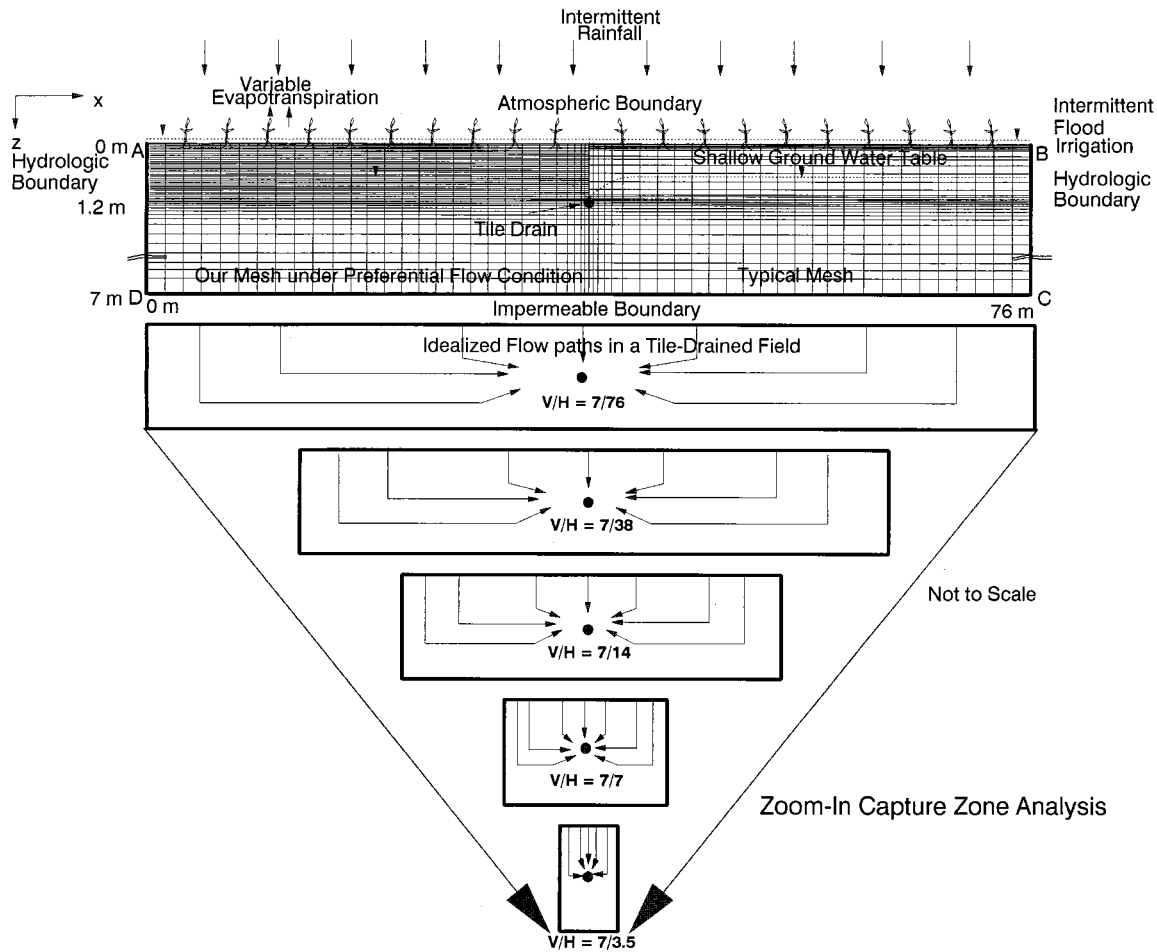
Figure 7. Typical/adapted finite element mesh including system-independent (time-dependent) and system-dependent flux/head-type atmospheric boundary, no-flux bottom and hydrologic boundaries, tile drain boundaries, and root water uptake sink for the two-dimensional flow/transport simulation in the vertical cross section of the field (study section) at Las Nutrias, New Mexico. The cross section of unit length (in Y direction) is assumed to be representative over the 240-m-long study section. Also shown is the step-zoom-in procedure adapted to study the capture zone of the tile drain.

interpolated water table elevation and NO_3^- concentration from the groundwater monitoring wells along the field boundary were used to define the initial conditions in the two-dimensional flow-transport domain Ω. In a few instances we used prior or posterior information to interpolate or extrapolate the data to our simulation starting date. Time-dependent boundary conditions, such as intermittent irrigation/precipitation rates and chemical application rates at atmospheric boundary nodes, groundwater head values along hydrologic boundary nodes, and no-flow conditions along impermeable bottom boundary nodes, were invoked. We simplified the two hydrologic boundaries (Γ_{AD} and Γ_{BC}, Figure 7) by assuming them to be impermeable (i.e., no regional flow contributions) during short-term irrigation-event-based simulations. The tile drain at the center of the study section was treated as a boundary node surrounded by four regular square elements with adjusted hydraulic conductivities using the electric analog approach of *Vimoke et al.* [1963] and *Fipps* [1986]. Mathematical details of the initial and boundary conditions for water flow at the field site are given by *Mohanty et al.* [1997].

For the long-term year-long simulation, we invoked an initial time step of one day with a starting date of March 1, 1994,

which coincided with our first soil sampling campaign at the Las Nutrias field site. As initial conditions we assumed the observed resident concentration for NO_3^- (C_{1994}), and zero concentrations for the other nitrogen species for all finite element nodes in the simulation domain Ω. For the short-term irrigation-event based simulations, we adopted 0.1-hour initial time steps and used the predicted soil water pressure heads and resident solute concentration ($c_k(x, z)$) levels at prespecified times from the long-term simulation as initial conditions. Given the specific field-hydrologic set-up and results of our experiment, this approach was found to be the best available option considering our objective of short-term high-frequency preferential flow predictions in the tile drain following flood irrigation.

Nitrogen fertilizer concentration of the irrigation/precipitation water was input as a Cauchy boundary condition across the top (soil-atmosphere) boundary, Γ_{AB}, of the flow-transport domain:

$$-\theta D_{ij} \frac{\partial c_k}{\partial x_j} n_i + q_i n_i c_k = q_i n_i c_{0,k} + \frac{D_g}{d} (k_g c_k - g_{atm}) \qquad (10)$$

$$(x, z) \in \Gamma_{AB} \quad k = 1 \cdots K \quad t \in t_{flux}$$

Table 6a. Field-Averaged Parameters of Bimodal Piecewise-Continuous and Unimodal van Genuchten-Mualem Hydraulic Functions for Different Soil Horizons at the Field Site near Las Nutrias, New Mexico

Depth, cm	Bimodal Piecewise-Continuous Hydraulic Functions						
	$\langle \theta_{s,i=1} \rangle$, cm^3 cm^{-3}	$\langle \theta_{r,i=1} \rangle$, cm^3 cm^{-3}	$\langle \alpha \rangle$, cm^{-1}	$\langle n \rangle$	$\langle K^* \rangle$, cm/s	$\langle h^* \rangle$, cm	$\langle \delta \rangle$, cm^{-1}
0–40	0.475	0.110	0.015	1.60	5.55E − 04	3	0.92
40–100	0.459	0.050	0.021	1.40	4.16E − 04	3	0.70
100–700	0.430	0.090	0.083	2.12	2.73E − 03	0	n/a

Depth, cm	Unimodal van Genuchten-Mualem Hydraulic Functions (High/Low)				
	$\langle \theta_s \rangle$, cm^3 cm^{-3}	$\langle \theta_r \rangle$, cm^3 cm^{-3}	$\langle \alpha \rangle$, cm^{-1}	$\langle n \rangle$	$\langle K_s \rangle$, cm/s
0–40	0.484/0.475	0.080/0.120	0.004/0.015	1.44/1.55	4.08E − 03/9.50E − 04
40–100	0.464/0.459	0.045/0.050	0.010/0.021	1.25/1.38	3.50E − 03/6.80E − 04
100–700	0.430/0.430	0.090/0.090	0.083/0.083	2.12/2.12	2.73E − 03/2.73E − 03

From *Mohanty et al*. [1997]. Read 5.55E−04 as 5.55×10^{-4}.

where $q_i n_i$ represents the outward fluid flux, n_i is the outward unit normal vector, $c_{0,k}$ is the concentration of the kth nitrogen species in the incoming fluid $[ML^{-3}]$, D_g is the molecular diffusion coefficient of nitrogen gas $[L^2 T^{-1}]$, d is the thickness of a stagnant boundary layer on the soil surface accounting for gas diffusion $[L]$ [*Jury et al*., 1983], g_{atm} is the nitrogen gas concentration in the atmosphere above the stagnant boundary layer $[ML^{-3}]$, and other variables are as defined earlier. For the impermeable bottom boundary, Γ_{CD}, and the hydrologic boundaries between adjacent tile lines (Γ_{BC}, Γ_{AD}), when ($q_i n_i = 0$), we used a Neumann boundary condition:

$$\theta D_{ij} \frac{\partial c_k}{\partial x_j} n_i = 0 \qquad (11)$$

$$(x, z) \in \Gamma_{CD} \vee \Gamma_{BC} \vee \Gamma_{AD} \quad k = 1 \cdots K \quad \forall t$$

Since a major focus of this study was on preferential flow that would occur during or relatively soon after flood irrigation, we limited the short-term simulation time to ~100 hours

Table 6b. Transport Parameters of Different Nitrogen Chain Products for Different Soil Horizons at the Field Site

Parameter	Chain Product	Depth, cm	Values of the Parameters
ρ, kg/m^3		0–40	1300
		40–100	1200
		100–700	1400
D_L, m		0–700	0.05
D_T, m		0–700	0.01
D^ω, m^2 h^{-1}		0–700	7.1×10^{-6}
D^g, m^2 h^{-1}		0–700	0.0
μ_ω, h^{-1}	NH$_4^+$	0–700	0.0005
μ_s, h^{-1}	NH$_4^+$	0–700	0.0005
μ_g, h^{-1}	NH$_4^+$	0–700	0.0
μ'_ω, h^{-1}	NH$_4^+$	0–700	0.005
μ'_ω, h^{-1}	NO$_2^-$	0–700	0.1
μ'_ω, h^{-1}	NO$_3^-$	0–700	0.0
μ'_s, h^{-1}	NH$_4^+$	0–700	0.005
μ'_s, h^{-1}	NO$_2^-$	0–700	0.0
μ'_s, h^{-1}	NO$_3^-$	0–700	0.0
μ'_g, h^{-1}	NH$_4^+$	0–700	0.0
μ'_g, h^{-1}	NO$_2^-$	0–700	0.0
μ'_g, h^{-1}	NO$_3^-$	0–700	0.0
γ_ω, h^{-1}	NO$_3^-$	0–700	0.002

from the start of an irrigation event. Also we adopted 0.1-hour (=6 min) initial time steps for our numerical simulations to closely follow the 5-min intervals of flow measurements in the field. The hydraulic parameters given in Table 6 were measured in the field [*Mohanty et al*., 1997]. The transport parameters for different solutes and soil types (Table 6) used in the numerical simulation were estimated from available literature [*van Genuchten*, 1985].

## 4. Simulation Results and Discussion

We present simulation results for four state variables. Figures 8 and 9 show predicted and observed water flow rates and NO$_3^-$ flux concentrations, respectively, in the tile drain for a typical irrigation event at the field site. The flow simulations were previously described by *Mohanty et al*. [1997]. In general, when the bimodal hydraulic functions were used, model predictions and observed data for tile flow matched reasonably well in magnitude. However, for different irrigation events, an early or delayed (e.g., Figure 8) predicted flow peak relative to the measured data was observed [*Mohanty et al*., 1997]. Furthermore, zero (westerly) flow was observed for several hours (e.g., hours 23 ~ 59, Figure 8) following every irrigation event. Also, observed water table levels in the adjacent monitoring
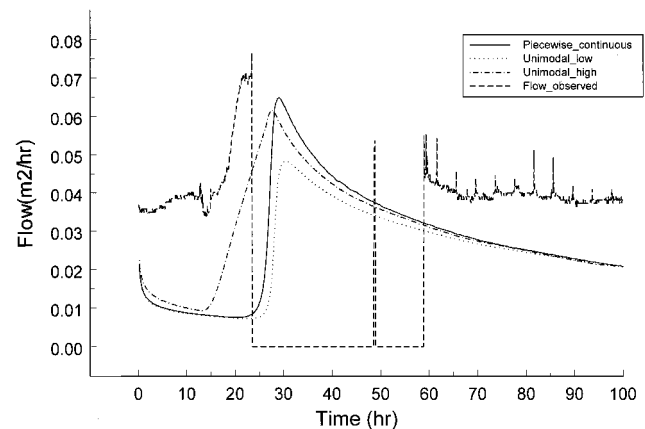
Figure 8. Comparison of predicted and observed tile flows following an irrigation event [after *Mohanty et al*., 1997].

wells and piezometers (not shown here) during and following a flood irrigation event revealed certain variations in the groundwater flow fields near the manholes warranting further investigation. We will discuss possible reasons for this unusual flow-transport behavior at our field site in the following sections.

Many earlier tile drainage studies neglected, for simplicity, the effects of a regional groundwater table gradient on the tile flow calculations. *Tod and Grismer* [1996] and *Singh and Kanwar* [1995a, b] indicated that the topographic and regional hydrologic conditions could well be a significant factor determining tile flow behavior. To investigate the significance of a regional ground water table gradient (at the field or bench scale), we analyzed data from two different dates with contrasting irrigation sequencing: the east-center-west bench (as defined in Table 1), August 24, 1995 (Figure 10a), and the west-center-east bench, September 7, 1995 (Figure 10b). Several factors (as shown in Figure 11) may contribute to the flow rate in the tile drain at a given time including factor a, the degree of submergence of the underdesigned tile drain below the water table (similar to observations by *Khan and Rushton* [1996b]); factor b, a regional (field-scale) groundwater table gradient across the three benches; factor c, a local groundwater table gradient immediately adjacent to the drain; and factor d, a bench-scale groundwater table gradient across the neighboring benches.

In a normal day between consecutive irrigation events, groundwater table showed a general northeast to approximately southwest gradient across the entire field and a local east to approximately west gradient near our study section (e.g., Figure 11b). Figure 10a shows that as water infiltrated during and following flooding of the east bench, the east tile drain became more submerged (factor a) and the east-to-center bench groundwater table gradient increased (factor d), thus increasing flow through both the east and west manholes. Apparently, this also resulted in a slight net loss of flow from the center bench due to the decreased local water table gradient there (factor c). Net center bench flow rates were determined simply by subtracting the flow measured in the east manhole from the flow measured in the west manhole. Afterward, subsequent to flooding and infiltration in the center bench, net flow rates increased for the same reasons as during
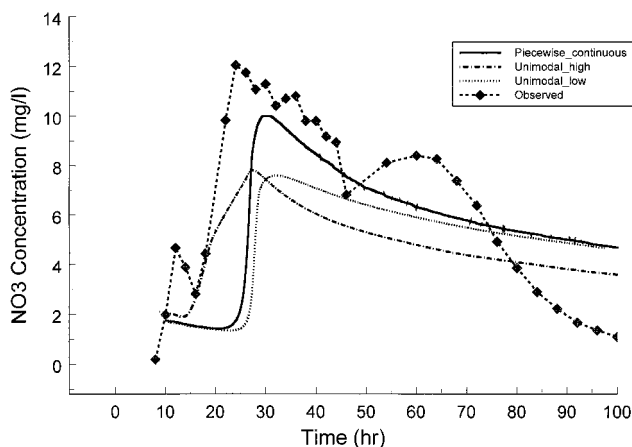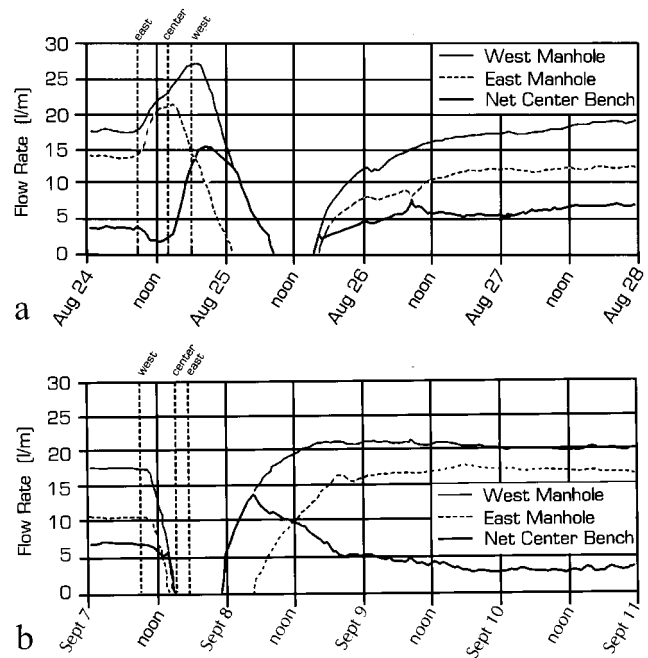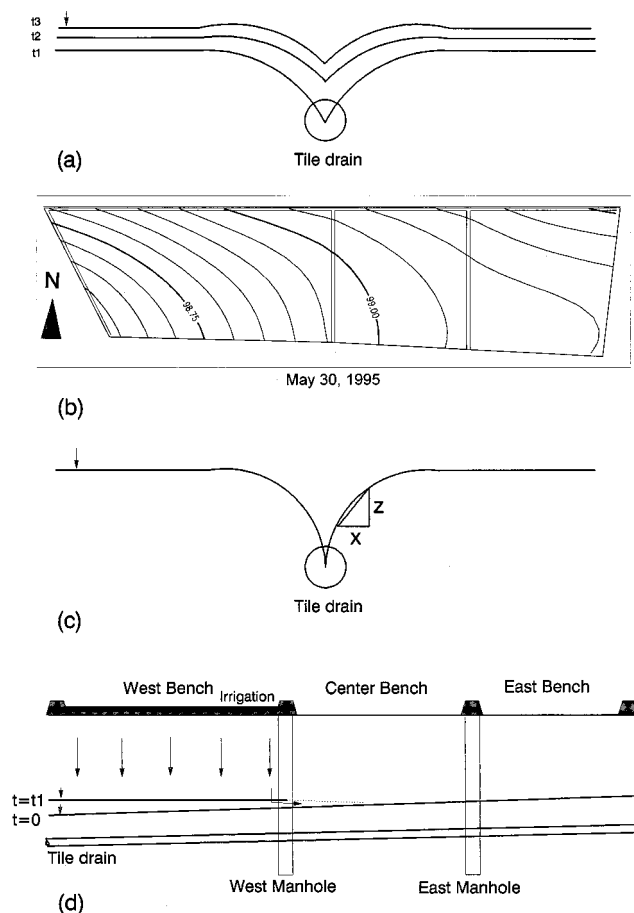

Figure 10. Typical tile flow behavior at the field site following (a) an east-center-west and (b) a west-center-east irrigation sequence. Vertical dashed lines represent irrigation starting times for the respective benches. Positive values indicate westerly flow. Occasional easterly flow are shown as zero flow.

flooding of east bench. However, flow rates from the east bench decreased as the east-to-center bench groundwater table gradient decreased (factor d). Eventually, flow rates from the east bench decreased to unmeasurable rates, and temporarily stagnated or even reversed direction (i.e., flow occurred from center to east bench). One-way valve of our flow meter could not register the amount of reverse flow thus simply indicating zero westerly flow. Subsequent to flooding and infiltration on the west bench, the center-to-west bench water table gradient was reduced (factor d), and net flow rates from the center bench declined rapidly to unmeasurable rates, which again stagnated or reversed direction (i.e., flow occurred from west to center bench). Unmeasurable flow rates in both the manholes persisted for a period of time until the east-to-west gradient (factor b) in the drain recovered sufficiently to establish measurable westerly flow rates.

For the west-to-east irrigation sequence (Figure 10b), following flooding and infiltration in the west bench, flow rates from the center and later the east bench rapidly stagnated or temporarily reversed because of west-east groundwater table gradient (factor b). Westerly flow was reestablished following flooding of the center and east benches. The observed peaks in the net center bench flow rate following the irrigation event are due to the recovery of measurable flow rates in the west manhole prior to their recovery in the east manhole. These findings suggest that tile flow and conservative (convection-dominated) solute transport in this field perhaps should have been better interpreted and modeled by means of a three-dimensional model that considers regional water and chemical management schemes (e.g., irrigation sequencing and fertilizer scheduling in neighboring benches) rather than the simplified two-dimensional approach used here for flow and transport to a tile drain.

Observed and predicted NO_3^- flux concentrations in the tile

Figure 9. Comparison of predicted and observed tile flux NO_3^- concentrations following the irrigation event on June 8, 1994, at the field site. Time 0 hour matches the midnight prior to the irrigation.

Figure 11. Factors contributing to transient tile flow-transport at our field site including (a) degree of submergence of the tile drain, (b) regional groundwater table gradient (e.g., groundwater table contour determined from 34 monitoring wells along the experimental field boundary on May 30, 1995), (c) local groundwater table gradient adjacent to the tile drain, and (d) bench-scale groundwater table gradient based on irrigation sequence of different field benches (e.g., west bench irrigation prior to center or east bench irrigation).

drain showed far better agreement when the bimodal hydraulic functions were used as compared to the unimodal van Genuchten-Mualem hydraulic functions (Figure 9). The most striking feature of Figure 9 is the presence of three peaks in the observed nitrate data. We believe that the peak concentration (~12 mg/L at hour 18) for this east-to-west irrigation event depicts field-scale preferential transport, while the peak (~9 mg/L at hour 60) is likely an artifact of the irrigation sequence and reverse flow as discussed in section 3. A smaller peak (~5 mg/L at hour 12) in NO_3^- concentration within ~3–4 hours from the start of the irrigation event likely occurred through a narrow zone above the tile drain, possibly because of soil disturbance during tile installation. Our piecewise-continuous hydraulic functions, however, could not fully distinguish between the three fast-flow regimes because of their lumped (continuum) nature. Moreover, following an irrigation event, simulated and observed NO_3^- flux concentration in the tile flow showed discrepancies of different degrees with time because of the same reasons of irrigation sequence and timing as for water flow. Piezometer NO_3^- concentrations (Figure 2) were somewhat over predicted by the model. In general, using the uni-

modal or bimodal hydraulic functions, the model predicts 2–3 times higher concentrations than the observed values. This result may be due to the assumption of impermeable hydrologic boundaries which neglect any mixing, dilution, and transport toward or from adjacent sites. Besides, uncertainties associated with the transport parameters of nitrogen species and other unrepresented nitrogen transformation processes may also contribute to these discrepancies.

Figure 12 shows predicted and measured field-averaged resident NO_3^- concentrations in the soil profile for the long-term simulation. Predicted field-averaged resident NO_3^- concentrations in the soil profile compared well to the corresponding field measured values. The model predictions were better for the shallow depths than for the deeper depths. We suggest that changes in the groundwater flow fields, as described earlier, may have been partly responsible for this depth-dependent behavior of resident NO_3^- concentration.

To verify the contribution of groundwater flow fields to the observed discrepancies in flux and resident NO_3^- concentrations, as well as in the tile flow volume, we conducted a step-zoom-in analyses for determining the tile drain capture zone during (preferential) peak and other peak flow periods. Also in a somewhat similar study in Indiana, *Kladivko et al.* [1991] found evidence of preferential flow to the tile drain originating in its close proximity. Keeping these findings in perspective, the step-zoom-in procedure was adopted by reducing the flow domain width in discrete steps, as shown in Figure 7. In each step, the flow domain was shrunk by approximately one half on both sides of the tile drain and the hydrologic boundaries between consecutive tile drains were assumed to match the modified flow transport domain boundaries. Hence hydrologic boundaries between consecutive tile drains spanned a finite length recharging to shallow groundwater that did not converge to any local tile drain (i.e., followed the regional groundwater flow path). For the step-zoom-in procedure we kept the depth
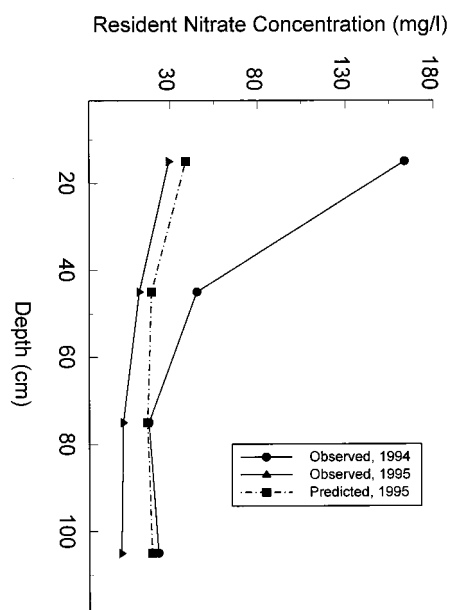
Figure 12. Comparison of predicted and observed (1995) field-averaged profile resident NO_3^- concentrations during the long-term simulation. Measured 1994 data were used as initial condition. Predictions (results) use bimodal hydraulic functions only.
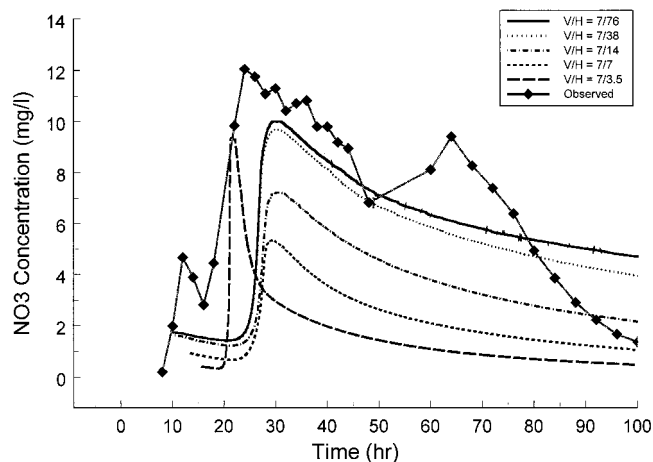
Figure 13. Comparison of tile flux NO_3^- concentrations for different effective capture lengths of the tile drain. The test case is for the irrigation event on June 8, 1994, at the field site.

of the flow domain constant (i.e., 7 m, up to the impermeable layer). This procedure resulted in five simulation runs with the flow domain width decreasing from 76 m up to 3.5 m.

By zooming in, flow fields gradually changed from three-dimensional (composite effect of local vertical seepage and regional groundwater flow) to two-dimensional local flow in close proximity of the tile drain (i.e., flow domain width of 3.5 m). Predicted tile flow NO_3^- flux concentration using the five selected domain widths (for June 8, 1994, east-center-west irrigation event) are presented in Figure 13. Apparently, a decrease in domain width to 3.5 m leads to somewhat better matches of the short-term model predictions to the observed nitrate concentration data in the tile drain at initial times (i.e., between hours 15 and 25). This finding suggests that during and immediately after an irrigation or heavy rainfall event, the tile drain located at 1.2-m depth at the field site is able to catch the flow and soluble NO_3^- from a narrow region adjacent to the tile drain. Assuming a somewhat similar mixing layer concept as used by *Shalit and Steenhuis* [1996], water during irrigation short-circuited horizontally from the irrigation ports via a network of surface-opened (shallow) cracks toward the tile drain and then infiltrated through the (disturbed) soil zone above the tile drains. Any chemical transported beyond this effective capture zone reached the groundwater table through some other pathways and eventually may or may not have reached the tile drains since nitrate reaching groundwater will undergo some denitrification by converting to N_2, N_2O, NO, and NO_2 under conditions of reduced oxygen supply.

Measured NO_3^- flux concentrations following the irrigation water application (between hours 25 and 40, Figure 13) matched reasonably well with the model prediction when using the full flow domain width of the tile drain (i.e., 76 m). In other words, during this period the total field width started contributing to the tile flow. Between hours 40 and 60 a dip in the tile flow NO_3^- concentration data reflects the typical reduced/reverse flow process during the east-center-west irrigation sequence as described earlier. In Figure 13, underpredictions and overpredictions in nitrate flux concentration beyond hour 60 are suggested to be associated with unrepresented nitrogen transport/transformation processes. Similar trends for tile flow NO_3^- concentrations and their match with model predictions were found for other irrigation events (not further shown

here), although peaks gradually reduced over time reflecting depletion (Figure 3).

The above findings relating to reduced/reverse flow also qualitatively agree with observations near the manholes and adjacent piezometric levels that the tile drain remained submerged during wet seasons. One of the reasons for this behavior is likely an underdesigned tile drain. In addition, the observed three-dimensional flow at the site as caused by the sequence and timing of irrigation of the three field benches (west to east or east to west) governed the field-scale hydrology and solute transport to the tile drain, resulting in some temporal shifts in the model predictions. Regional groundwater gradients in our two-dimensional flow-transport model were represented by monthly head values (for long-term simulations) at hydrologic divides across the study section. Boundary conditions of this type were found to be too crude to catch the effect of field-scale hydrology on tile flow following any short-term flood irrigation event. Hence, on the basis of our field-monitoring program, our mathematical modeling, and our data analyses, we infer that tile drains do not necessarily provide a good integrated representation of field-scale flow/transport behavior, in particular when the tiles are underdesigned and/or the hydrology at the field site is three-dimensional. Regional hydrology may also be a significant factor, in addition to the local hydrology. However, tile drains still should be useful for catching preferential flow phenomena from areas close to the drains, following any heavy water input event. We conclude that the proposed model based on CHAIN_2D and using piecewise-continuous hydraulic functions appears to be an appropriate tool for making flow-transport prediction in tile-drained fields.

References

Booltink, H. W. G., Field monitoring of nitrate leaching and water flow in a structured clay soil, *Agric. Ecosyst. Environ.*, *52*(2–3), 251–261, 1995.

Bowman, R. S., and R. C. Rice, Transport of conservative tracers in the field under intermittent flood irrigation, *Water Resour. Res.*, *22*, 1531–1536, 1986.

Celia, M. A., E. T. Bouloutas, and R. L. Zabra, A general mass-conservative numerical solution for the unsaturated flow equation, *Water Resour. Res.*, *26*, 1483–1496, 1990.

Czapar, G. F., and R. S. Kanwar, Field measurement of preferential flow using subsurface drainage tiles, paper presented at Preferential Flow Symposium, Am. Soc. of Agric. Eng., St. Joseph, Mich., 1991.

Feddes, R. A., E. Bresler, and S. P. Neuman, Field test of a modified numerical model for water uptake by root systems, *Water Resour. Res.*, *10*, 1199–1206, 1974.

Feddes, R. A., P. J. Kowalik, and H. Zaradny, *Simulation of Field Water Use and Crop Yield*, John Wiley, New York, 1978.

Fipps, G., R. W. Skaggs, and J. L. Nieber, Drains as a boundary condition in finite elements, *Water Resour. Res.*, *22*, 1613–1621, 1986.

Hallberg, G. R., J. L. Baker, and G. W. Randall, Utility of tile-line effluent studies to evaluate the impact of agricultural practices on groundwater, paper presented at Agricultural Impacts on Ground Water Conference, Natl. Water Well Assoc., Dublin, Ohio, 1986.

Huang, K., B. P. Mohanty, and M. T. van Genuchten, A new convergence criterion for the modified picard iteration method to solve the variably saturated flow equation, *J. Hydrol.*, *178*, 69–91, 1996.

Journel, A. G., and C. J. Huijbregts, *Mining Geostatistics*, 600 pp., Academic, San Diego, Calif., 1978.

Jury, W. A., Solute travel-time estimates for tile-drained fields, I, Theory, *Soil Sci. Soc. Am. J.*, *39*, 1020–1024, 1975a.

Jury, W. A., Solute travel-time estimates for tile-drained fields, II, Application to experimental studies, *Soil Sci. Soc. Am. J.*, *39*, 1024–1028, 1975b.

Jury, W. A., W. F. Spencer, and W. J. Farmer, Behavior assessment model for trace organics in soil, I, Model description, *J. Environ. Qual.*, *12*, 558–564, 1983.

Kamra, S. K., S. R. Singh, K. V. G. K. Rao, and M. T. van Genuchten, A semidiscrete model for water and solute movement in tile-drained soils, 1, Governing equations and solution, *Water Resour. Res.*, *27*, 2439–2447, 1991a.

Kamra, S. K., S. R. Singh, K. V. G. K. Rao, and M. T. van Genuchten, A semidiscrete model for water and solute movement in tile-drained soils, 2, Field validation and applications, *Water Resour. Res.*, *27*, 2449–2456, 1991b.

Khan, S., and K. R. Rushton, Reappraisal of flow to tile drains, II, Time-variant response, *J. Hydrol.*, *183*, 367–382, 1996a.

Khan, S., and K. R. Rushton, Reappraisal of flow to tile drains, III, Drains with limited flow capacity, *J. Hydrol.*, *183*, 383–395, 1996b.

Kladivko, E. J., G. E. Van Scoyoc, E. J. Monke, K. M. Oates, and W. Pask, Pesticides and nutrient movement into tile drains on a silt loam soil in Indianan, *J. Environ. Qual.*, *20*, 264–270, 1991.

Luxmoore, R. J., On preferential flow and its measurement, paper presented at Preferential Flow Symposium, Am. Soc. of Agric. Eng., St. Joseph, Mich., 1991.

Mohanty, B. P., R. S. Bowman, J. M. H. Hendrickx, and M. T. van Genuchten, New piecewise-continuous hydraulic functions for modeling preferential flow in an intermittent-flood-irrigated field, *Water Resour. Res.*, *33*, 2049–2063, 1997.

Munster, C. L., R. W. Skaggs, J. E. Parsons, R. O. Evans, J. W. Gilliam, and M. A. Breve, Simulating Aldicrab transport in a drained field, *Trans. ASAE*, *37*, 1817–1824, 1994.

Munster, C. L., R. W. Skaggs, and V. R. Pemmireddy, Effect of water table management on the fate of the pesticide Aldicrab, *Trans. ASAE*, *39*, 55–66, 1996.

National Resource Conservation Service (NRCS), Soil survey map of Las Nutrias, New Mexico, Lincoln, Neb., 1992.

Nielsen, D. R., and J. G. MacDonald (Ed.), *Nitrogen in the Environment*, vol. 2, 528 pp., Academic, San Diego, Calif., 1978.

Novotny, V., and G. Chesters, *Handbook of Nonpoint Pollution*, 555 pp., van Nostrand Reinhold, New York, 1981.

Perrochet, P., and D. Berod, Stability of the standard Crank-Nicolson-Galerkin scheme applied to the diffusion-convection equation: Some new insights, *Water Resour. Res.*, *29*, 3291–3297, 1993.

Ragab, R., D. M. Cooper, G. L. Harris, and J. A. Catt, Simulating nitrate under winter wheat grown on a structured clay soil considering bypass flow, *J. Hydrol.*, *182*, 157–173, 1996.

Richard, T. L., and T. S. Steenhuis, Tile drain sampling of preferential flow on a field scale, *J. Contam. Hydrol.*, *3*, 307–325, 1988.

Samani, Z., Measuring water in trapezoidal canals, *J. Irrigat. Drain. Eng.*, *119*, 181–186, 1993.

Sanoja, J., R. S. Kanwar, and S. W. Melvin, Comparison of simulated (DRAINMOD) and measured tile outflow and water table elevations from two field sites in Iowa, *Trans. ASAE*, *33*, 827–833, 1990.

Shalit, G., and T. Steenhuis, A simple mixing layer model predicting solute flow to drainage lines under preferential flow, *J. Hydrol.*, *183*, 139–149, 1996.

Shapiro, S. S., and W. B. Wilk, An analysis of variance test for normality (complete examples), *Biometrika*, *52*, 591–611, 1965.

Simunek, J., and M. T. van Genuchten, The CHAIN_2D code for simulating the two-dimensional movement of water, heat, and multiple solutes in variably-saturated porous media, *Res. Rep. 136*, U.S. Salinity Lab., Riverside, Calif., 1994.

Singh, P., and R. S. Kanwar, Modification of RZWQM for simulating subsurface drainage by adding a tile flow component, *Trans. ASAE*, *38*, 489–498, 1995a.

Singh, P., and R. S. Kanwar, Simulating NO_3-N transport to subsurface drain flows as affected by tillage under continuous corn using modified RZWQM, *Trans. ASAE*, *38*, 499–506, 1995b.

Singh, P., R. S. Kanwar, K. E. Johnsen, and L. R. Ahuja, Calibration and evaluation of subsurface drainage component of RZWQM v. 2.5, *J. Environ. Qual.*, *25*, 56–63, 1996.

Thomas, G. W., and B. J. Barfield, The unreliability of tile effluent for monitoring subsurface nitrate-nitrogen losses from soils, *J. Environ. Qual.*, *3*, 183–185, 1974.

Tod, I. C., and M. E. Grismer, Issues confronting salinity and drainage management in irrigated agriculture, *USCID Newsl.*, pp. 4–5, U.S. Comm. on Irrigat. and Drain., Denver, Colo., Jan.–July 1996.

van Genuchten, M. T., A closed-form equation for predicting the hydraulic conductivity of unsaturated soils, *Soil Sci. Soc. Am. J.*, *44*, 892–898, 1980.

van Genuchten, M. T., Convective-dispersive transport of solutes involved in sequential first-order decay reactions, *Comput. Geosci.*, *11*, 129–147, 1985.

Vimoke, B. S., and G. S. Taylor, Simulating water flow in soil with an electric resistance network, *Res. Rep. 41-65*, Soil and Water Conserv. Res. Div., U.S. Dep. of Agric., Agric. Res. Serv., Columbus, Ohio, 1962.

Vimoke, B. S., T. D. Tura, T. J. Thiel, and G. S. Taylor, Improvements in construction and of resistance networks for studying drainage problems, *Soil Sci. Soc. Am. Proc.*, *26*, 203–207, 1963.

White, R. E., S. R. Wellings, and J. P. Bell, Seasonal variations in nitrate leaching in structured clay soils under mixed land use, *Agric. Water Manage.*, *7*, 391–410, 1983.

Yeh, G. T., and V. S. Tripathi, HYDROGEOCHEM: A coupled model of HYDROlogic transport and GEOCHEMical equilibria in reactive multicomponent systems, *Publ. 3170*, Environs Sci. Div., Oak Ridge Natl. Lab., Oak Ridge, Tenn., 1990.

R. S. Bowman and J. M. H. Hendrickx, Department of Earth and Environmental Sciences, New Mexico Institute of Mining and Technology, Socorro, NM 87801.

B. P. Mohanty, J. Simunek, and M. T. van Genuchten, U.S. Salinity Laboratory, 450 W. Big Springs Road, Riverside, CA 92507. (e-mail: bmohanty@ussl.ars.usda.gov)